PROCEEDINGS OF SCIENCE

An a_0 resonance in strongly coupled $\pi\eta$, $K\overline{K}$ scattering from lattice QCD

Jozef Dudek[*†]

Department of Physics, College of William and Mary, Williamsburg, VA 23187, USA
Jefferson Lab, 12000 Jefferson Avenue, Newport News, VA 23606, USA

E-mail: dudek@jlab.org

Scattering amplitudes for the coupled-channels $\pi\eta$, $K\overline{K}$ and $\pi\eta'$ in isospin $= 1$ are extracted from the discrete spectrum of eigenstates in three volumes determined using lattice QCD with $m_\pi = 391$ MeV. The S-wave is found to feature a prominent cusp-like structure in $\pi\eta \to \pi\eta$ close to $K\overline{K}$ threshold, and an $a_0(980)$-like resonance is identified, corresponding to a pole in the complex energy plane, coupled to both $\pi\eta$ and $K\overline{K}$.

34^{th} *annual International Symposium on Lattice Field Theory*
24-30 July 2016
University of Southampton, UK

[*]Speaker.
[†]for the Hadron Spectrum Collaboration

1. Introduction

The excited spectroscopy of QCD is the study of *resonances* – excited hadrons are not asymptotic states, they decay rapidly to lighter stable hadrons, and appear in experiments as enhancements in the scattering of these stable hadrons. It follows that to rigorously study the excited spectrum of QCD we should calculate *scattering amplitudes* and examine their resonant content. The presence of a resonance is signaled by the scattering amplitude having a *pole singularity* at a complex value of the scattering energy.

Using lattice QCD we can calculate Euclidean two-point correlation functions using operators having the quantum numbers of the hadronic scattering channels we're interested in. The time-dependence of these correlation functions is controlled by the discrete spectrum of QCD eigenstates within the finite cubic volume defined by the lattice boundary.

A formalism exists which relates the discrete spectrum in a finite cubic volume to infinite volume hadron-hadron scattering amplitudes [1]. This formalism has been widely applied in the case of elastic P-wave $\pi\pi$ scattering where the ρ resonance resides [2, 3, 4, 5]. Detailed studies determine the spectrum in multiple volumes and/or in several moving frames, leading to the elastic scattering phase-shift being mapped out in detail [6, 7].

There has, however, been only limited consideration of the more generally applicable case of resonances in coupled-channels, i.e. where a resonance can decay to more than a single final state. The first explicit lattice QCD calculation [8, 9] considered the coupled $\pi K, \eta K$ system, but this proved to be only weakly coupled, with resonances appearing dominantly coupled to only the πK channel.

This proceedings (and a longer paper [10]) reports on the first study of a strongly coupled-channel system, that of $\pi\eta, K\overline{K}$. In this case, experimentally, we know that the S-wave contains a low-lying resonance, the $a_0(980)$, which manifests as a sharp enhancement at the $K\overline{K}$ threshold, coupled to both $\eta\pi$ and $K\overline{K}$ channels.

2. Computing the spectrum

We obtain discrete spectra by analyzing matrices of correlations functions computed using a basis of operators built from two basic types: "single-hadron-like" operators, $\overline{\psi}\Gamma D\ldots D\psi$, projected into definite momentum and into the relevant irreducible representations of the lattice symmetry group, and "meson-meson-like" operators.

The "meson-meson-like" constructions that we utilize take the form $\sum_{\vec{p}_1,\vec{p}_2}\mathscr{C}(\vec{p}_1,\vec{p}_2)\,\Omega^\dagger(\vec{p}_1)\,\Omega^\dagger(\vec{p}_2)$, where $\Omega^\dagger(\vec{p})$ is a variationally-optimal momentum-projected operator [11] that is obtained as a linear superposition of the "single-hadron-like" basis for each of the π, K, η and η'. We combine these with the Clebsch-Gordon coefficients for the desired lattice irrep to produce "$\pi\eta$-like", "$K\overline{K}$-like" and "$\pi\eta'$-like" operators in the manner described in Ref. [12].

Calculating correlation functions using these operators requires evaluating a number of different Wick contractions, including several which feature $q\bar{q}$ annihilation. All such diagrams are computed without further approximation using the *distillation* quark smearing framework, which also has the advantage of factorizing the operator construction from the quark propagation – as such the same quark propagation objects can be reused in a range of scattering calculations.

We analyze the resulting correlation matrices using a variational method which amounts to solving a generalized eigenvalue problem of the form $C(t)v^{\mathrm{n}} = C(t_0)v^{\mathrm{n}}\lambda_{\mathrm{n}}(t)$, where the spectrum of eigenstates, $\{E_{\mathrm{n}}\}$, is obtained from the large time behavior of the "principal correlators", $\lambda_{\mathrm{n}}(t) \sim e^{-E_{\mathrm{n}}(t-t_0)}$.

Fig. 1 illustrates the low energy part of the spectrum in the rest frame determined on three lattice volumes. The histograms show the relative overlap strengths for each state with operators of the various types described above. We see that a diverse basis of operators allows the states to be clearly distinguished in the space explored by the variational solution.

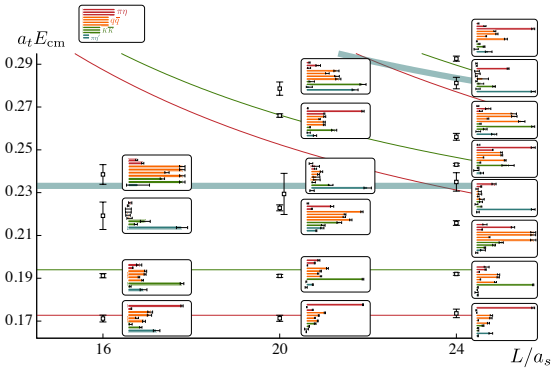

Figure 1: Spectra in the rest frame A_1 irrep on three volumes. Curves show the non-interacting $\pi\eta$(red), $K\overline{K}$(green) and $\pi\eta'$(blue) energy levels. The histograms indicate the normalized overlap of each state onto each operator in the variational basis, illustrating the need for such a broad basis to extract the variety of observed levels.

We obtain significant constraint on the scattering amplitudes by determining spectra in a range of frames moving with respect to the lattice – we are careful in these cases to construct operators which are irreducible under the reduced "little-group" symmetry [11]. A subset of the calculated spectra are shown in Fig. 2, where we observe that there are energy levels covering the whole region from slightly below $\pi\eta$ threshold to around the $\pi\eta'$ threshold.

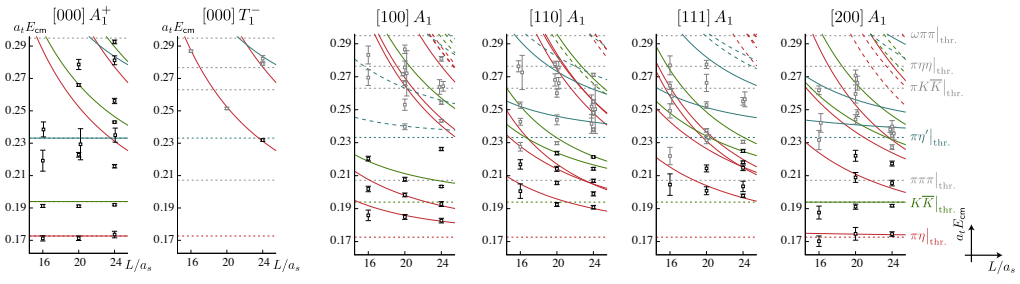

Figure 2: Spectra on three volumes in various rest-frame and moving-frame irreps. All except $[000]\,T_1^-$ have S-wave scattering as their leading contribution. The lack of deviation from the non-interacting curves in $[000]\,T_1^-$ indicates the absence of significant scattering in the P-wave (which has exotic $J^{PC} = 1^{-+}$ quantum numbers) at low energies.

3. Coupled-channel scattering amplitudes

The relation between finite volume spectra and infinite volume scattering amplitudes is provided within the formalism first derived for elastic scattering by Lüscher [1, 13], with later extensions to allow for moving frames, non-zero spin, and scattering of particles of unequal mass.

In the case of *coupled-channel* hadron-hadron scattering described by the scattering t-matrix, $\mathbf{t}(E_{\mathsf{cm}})$, the corresponding finite-volume formalism [14, 15, 16, 17, 18] can be written,

$$\det[\mathbf{1} + i\boldsymbol{\rho}\cdot\mathbf{t}\cdot(\mathbf{1} + i\mathscr{M})] = 0, \tag{3.1}$$

with $\boldsymbol{\rho}(E_{\mathsf{cm}})$ the phase-space matrix and $\mathscr{M}(E_{\mathsf{cm}}, L)$ a matrix of known functions diagonal in the scattering channel space. The finite-volume spectrum in a cubic $L\times L\times L$ volume, corresponds to the set of solutions, $\{E_{\mathsf{cm}}(\mathfrak{n})\}$, of Eq. 3.1, for a unitarity-preserving $\mathbf{t}(E_{\mathsf{cm}})$.

The K-matrix approach is convenient in that it ensures that the t-matrix is unitarity-preserving. In general, for ℓ-wave scattering, the relation between K and t is,

$$t_{ij}^{-1}(s) = \frac{1}{(2k_i)^\ell} K_{ij}^{-1}(s) \frac{1}{(2k_j)^\ell} + I_{ij}(s)\,, \tag{3.2}$$

where the factors $(2k_i)^{-\ell}$ provide the required kinematic behavior at thresholds. The elements $K_{ij}(s)$ form a symmetric matrix that is real for real $s = E_{\mathrm{cm}}^2$. The elements $I_{ij}(s)$ form a diagonal matrix whose imaginary part is fixed by unitarity to be $-\rho_i(s)$ above threshold in channel i and zero below threshold. A convenient choice for $I(s)$, having good analytic properties, is the "Chew-Mandelstam" phase space (described in the appendices of Ref. [9]). We will explore a range of parameterizations for $\mathbf{K}(s)$ when we consider coupled-channel scattering to ensure that the results are not dependent on any particular choice.

One simple implementation which describes the spectra of Fig. 2 very well up to the $\pi\eta'$ threshold, parameterizes the two-channel K-matrix as a pole plus a matrix of constants,

$$\mathbf{K} = \frac{1}{m^2 - s}\begin{bmatrix} g_{\pi\eta}^2 & g_{\pi\eta}g_{K\bar{K}} \\ g_{\pi\eta}g_{K\bar{K}} & g_{K\bar{K}}^2 \end{bmatrix} + \begin{bmatrix} \gamma_{\pi\eta,\pi\eta} & \gamma_{\pi\eta,K\bar{K}} \\ \gamma_{\pi\eta,K\bar{K}} & \gamma_{K\bar{K},K\bar{K}} \end{bmatrix}, \tag{3.3}$$

where the six real parameters, m, $g_{\pi\eta}$, $g_{K\bar{K}}$, $\gamma_{\pi\eta,\pi\eta}$, $\gamma_{\pi\eta,K\bar{K}}$, $\gamma_{K\bar{K},K\bar{K}}$, can be varied and the best description of the finite-volume spectra is given by parameter values

$$\begin{aligned} a_t\, m &= (0.2214 \pm 0.0029 \pm 0.0004) \\ a_t\, g_{\pi\eta} &= (\ 0.091 \pm 0.016 \pm 0.009) \\ a_t\, g_{K\bar{K}} &= (-0.129 \pm 0.015 \pm 0.002) \\ \gamma_{\pi\eta,\pi\eta} &= -0.16 \pm 0.24 \pm 0.03 \\ \gamma_{\pi\eta,K\bar{K}} &= -0.56 \pm 0.29 \pm 0.04 \\ \gamma_{K\bar{K},K\bar{K}} &= \ 0.12 \pm 0.38 \pm 0.08 \end{aligned} \qquad \begin{bmatrix} 1 & 0.58 & -0.06 & -0.51 & 0.39 & 0.02 \\ & 1 & -0.63 & -0.87 & 0.84 & -0.49 \\ & & 1 & 0.52 & -0.68 & 0.83 \\ & & & 1 & -0.90 & 0.53 \\ & & & & 1 & -0.78 \\ & & & & & 1 \end{bmatrix}$$

$$\chi^2/N_{\mathrm{dof}} = \tfrac{58.0}{47-6} = 1.41\,, \tag{3.4}$$

where the uncertainties are first statistical and second due to variation of m_π, m_K, m_η and the anisotropy of the lattice, ξ, within their uncertainties. The matrix shows the parameter correlations.

Plotting quantities proportional to cross-sections, in the left panel of Fig. 3, we see a prominent cusp structure in $\pi\eta \to \pi\eta$ at the opening of the $K\overline{K}$ threshold, and a rapid turn of processes leading to the $K\overline{K}$ final state. An alternative presentation of the t-matrix uses phase-shifts for each channel and an inelasticity parameter[1] as shown in the right panel of Fig. 3. The inelasticity deviates sharply from unity at $K\overline{K}$ threshold indicating the large coupling between channels.

In Fig. 3 the inner error band reflects the statistical uncertainty propagated through from the finite volume-energy levels, while the outer error band indicates the maximum 1σ deviations we encounter while considering a much larger variety of parameterization forms (a full list is presented in Ref. [10]). We clearly see that it is the finite-volume energy levels which are determining the energy-dependence of the amplitudes and not the particular choice of parameterization form.

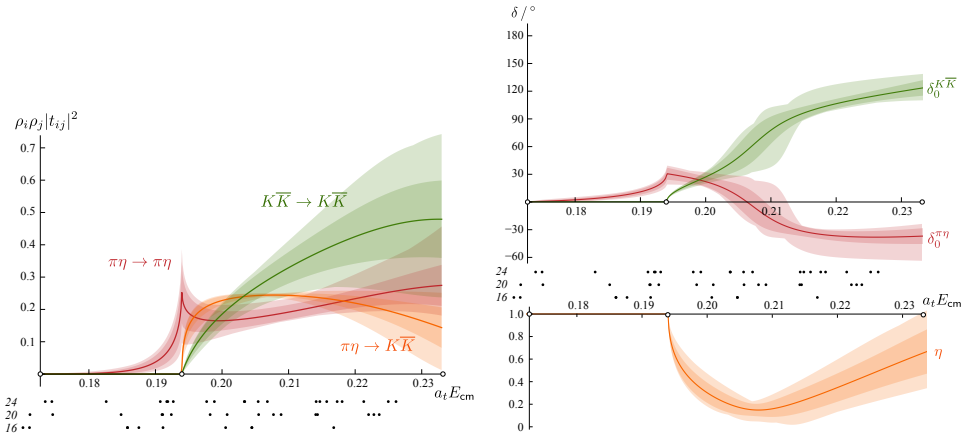

Figure 3: (left) Quantity proportional to cross-section. Curves and innermost errorbands show the result of the fit given by Eqn. 3.4. Outermost errorbands indicate the 1σ deviation when considering a much wider range of possible parameterizations. (right) Same amplitudes expressed as two-channel phase-shifts and inelasticity.

A cusp at the opening of a new threshold is a general feature, caused by the square root branch-point singularity at the threshold, but the strength of the effect in Fig. 3 in unlikely to be due to this alone. The very rapid turn-on of the $K\overline{K}$ amplitudes suggests that there may well be resonant behavior in this energy region and in the next section we will examine the continuation of our amplitudes to complex values of s to determine if there are nearby pole singularities that may provide a resonant explanation of the above observations.

4. Resonance poles

The scattering amplitudes that we have extracted are directly constrained for real values of $s = E_{\rm cm}^2$ by the finite-volume energy levels computed in our lattice QCD calculations. In a similar way, scattering amplitudes may be determined experimentally using scattering data collected at real energies above kinematic thresholds. It has proven useful to consider the continuation of these amplitudes to values of s in the complex plane since singularities, in particular pole singularities associated with resonances, are the dominating features.

[1] The S-matrix is given by $\mathbf{S} = \mathbf{1} + 2i\sqrt{\rho}\cdot\mathbf{t}\cdot\sqrt{\rho}$, with diagonal elements of S being $\eta\, e^{2i\delta_{\pi\eta}}, \eta\, e^{2i\delta_{K\bar{K}}}$

The structure of the complex s-plane away from the real axis becomes more complicated as new scattering channels open. Each new square-root branch-cut associated with an opening threshold splits the plane into two Riemann sheets, so that for n-channel scattering, there are 2^n sheets. In the two channel region there are four sheets to consider, and they may be labelled by the sign of the imaginary part of the cm-frame momenta for the two channels:

Sheet	I	II	III	IV
$\mathrm{Im}\,k_{\pi\eta}$	$+$	$-$	$-$	$+$
$\mathrm{Im}\,k_{K\overline{K}}$	$-$	$+$	$-$	$-$

Physical scattering occurs on sheet I, just above the real s axis where the branch cuts that lead to the other, "unphysical", sheets lie. Causality ensures that singularities cannot appear off the real axis on the physical sheet, but they can appear on any of the unphysical sheets. In particular, we can have poles at complex values of s, and in a region near a pole we have for an element of the t-matrix, $t_{ij} \sim \frac{c_i c_j}{s_0 - s}$. s_0 is the pole position, which is often associated with a resonance mass and width as $s_0 = \left(m_R \pm \frac{i}{2}\Gamma_R\right)^2$, and the residue can be factorized into c_i, c_j, couplings that indicate the relative strength with which the pole couples to each channel.

We examined the singularity structure of the amplitudes that were found to be capable of describing the finite-volume spectra, and the pole positions are presented in Figure 4. In every case we find a pole on IV$_u$ located rather close to the real axis slightly above the $K\overline{K}$ threshold (red points). The distribution of other (relatively) nearby poles depends strongly upon the parameterization – typically we find a III$_l$ pole located significantly further into the complex plane (blue points), and we see that its position varies significantly with parameterization choice. The (green) pole on the real axis is on sheet III or IV and is far from the $\pi\eta$ threshold.

The right panel of Figure 4 makes it clear that the well-determined IV$_u$ pole is actually very close to II$_l$, these two sheets being continuously connected. It is also clear that a pole at this position is likely to strongly influence the behavior of amplitudes close to the $K\overline{K}$ threshold, while the poorly determined pole on sheet III is most likely influencing the higher energy behavior of the amplitudes.

In [10], an additional study using Jost functions was presented – this allowed the number and position of pole singularities to be controlled explicitly. The conclusion of this study was that the sheet IV pole is required to explain the threshold behavior, while the other singularities play a relatively minor role.

The sheet IV pole in the t-matrix has a residue that factorizes into couplings to the $\pi\eta$ and $K\overline{K}$ channels of roughly equal magnitude, indicating the strong coupling of the channels through this resonance.

5. Summary

We have presented the first extraction of a strongly coupled-channel meson-meson scattering system in lattice QCD finding an S-wave resonance which may be associated with the experimental $a_0(980)$ state. The resonance we find lies in the two coupled-channel ($\pi\eta$, $K\overline{K}$) region, appearing as a cusp-like structure at $K\overline{K}$ threshold associated with a single pole on the IV Riemann sheet. A more detailed discussion of the work described here can be found in [10].

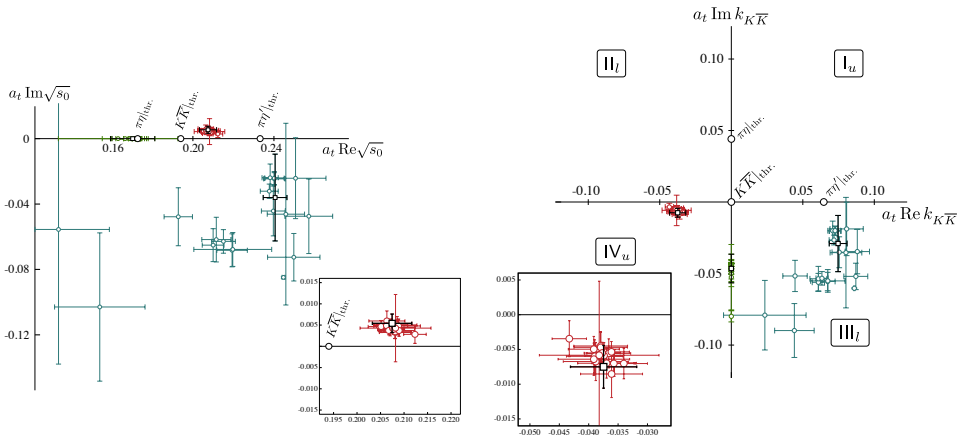

Figure 4: Pole singularities found in parameterized descriptions of the finite-volume spectra. (left) Complex energy plane with red points on sheet IV, blue points on sheet III. The black points indicate the poles found for the description given in Eqn. 3.4. (right) The same poles plotted in the complex $k_{K\overline{K}}$ plane, which makes it clear that the (red) pole on sheet IV is the one controlling the behavior of the amplitude at $K\overline{K}$ threshold.

References

[1] M. Lüscher, *Nucl.Phys.* **B354** (1991) 531–578.

[2] G. S. Bali, S. Collins, A. Cox, G. Donald, M. Gockeler, C. B. Lang et al., 1512.08678.

[3] S. Aoki et al., *Phys. Rev.* **D84** (2011) 094505, [1106.5365].

[4] X. Feng, K. Jansen and D. B. Renner, *Phys. Rev.* **D83** (2011) 094505, [1011.5288].

[5] S. Aoki et al., *Phys. Rev.* **D76** (2007) 094506, [0708.3705].

[6] J. J. Dudek, R. G. Edwards and C. E. Thomas, *Phys. Rev.* **D87** (2013) 034505, [1212.0830].

[7] D. J. Wilson et al., *Phys. Rev.* **D92** (2015) 094502, [1507.02599].

[8] J. J. Dudek et al., *Phys. Rev. Lett.* **113** (2014) 182001, [1406.4158].

[9] D. J. Wilson et al., *Phys. Rev.* **D91** (2015) 054008, [1411.2004].

[10] J. J. Dudek, R. G. Edwards and D. J. Wilson, *Phys. Rev.* **D93** (2016) 094506, [1602.05122].

[11] C. E. Thomas, R. G. Edwards and J. J. Dudek, *Phys. Rev.* **D85** (2012) 014507, [1107.1930].

[12] J. J. Dudek, R. G. Edwards and C. E. Thomas, *Phys. Rev.* **D86** (2012) 034031, [1203.6041].

[13] M. Lüscher, *Nucl.Phys.* **B364** (1991) 237–254.

[14] S. He, X. Feng and C. Liu, *JHEP* **0507** (2005) 011, [hep-lat/0504019].

[15] P. Guo, J. Dudek, R. Edwards and A. P. Szczepaniak, *Phys. Rev.* **D88** (2013) 014501, [1211.0929].

[16] M. T. Hansen and S. R. Sharpe, *Phys.Rev.* **D86** (2012) 016007, [1204.0826].

[17] R. A. Briceno and Z. Davoudi, *Phys. Rev.* **D88** (2013) 094507, [1204.1110].

[18] R. A. Briceno, *Phys.Rev.* **D89** (2014) 074507, [1401.3312].